Eur. Phys. J. Appl. Phys. **86**, 11301 (2019)

https://doi.org/10.1051/epjap/2019190013

THE EUROPEAN PHYSICAL JOURNAL APPLIED PHYSICS

Regular Article

The growth of silver nanostructures on porous silicon for enhanced photoluminescence: The role of $AgNO_3$ concentration and deposition time

Alper Cetinel[1,*], Nurcan Artunç[1], and Enver Tarhan[2]

[1] Department of Physics, Ege University, Bornova 35100, Izmir, Turkey
[2] Department of Physics, Izmir Institute of Technology, Urla 35430, Izmir, Turkey

Received: 18 January 2019 / Received in final form: 8 April 2019 / Accepted: 3 May 2019

Abstract. Silver nanostructures were obtained by using the electrodeposition method on n-type porous silicon (PSi) under different deposition times and concentrations of $AgNO_3$ solutions. The analyses of the structural and photoluminescence properties of PSi/Ag were studied by SEM, XRD and photoluminescence spectroscopy. SEM analysis showed that the shape and size of Ag nanostructures significantly depend on the deposition time and concentration. It was found that spherical nanoparticles and thin Ag dendrites were obtained in short deposition times at 1 and 5 mM $AgNO_3$ concentrations, whereas, Ag complex dendrite nanostructures formed in long deposition times. It was also found that only micro-sized Ag particles were formed at 10 mM. XRD results revealed that the degree of crystallization increases with increasing concentration. Photoluminescence analysis showed that the deposition time and concentration of $AgNO_3$ remarkably affect the PL intensity of PSi/Ag samples. We determined a PL enhancement of ~2.7 for the PSi/Ag deposited at 120 s for 1 mM $AgNO_3$. The improved PL intensity of PSi/Ag nanostructures can be explained by the combination of quantum confinement and surface states. PL analyses also indicated that with increasing deposition time and $AgNO_3$ concentrations, the PL intensity of PSi/Ag structures significantly decreases due to the auto-extinction phenomenon.

1 Introduction

There has been much talk of porous silicon (PSi) in recent years because of tunable room temperature visible light emission from PSi. In addition to its unique photoluminescence properties, the extremely large surface area, the ease of its formation and controllability of the surface morphology of PSi have drawn considerable attention for use in potential applications in optoelectronics, chemical sensing and biomedical fields [1]. But, as well known, the metastable silicon–hydrogen (Si–H) bonds in PSi matrix are easily broken by oxygen in the ambient atmosphere which results in the degradation of surface chemistry and instability of optical characteristic in PSi [2]. Due to the outstanding instability problem of PSi, passivation of its surface is necessary to develop porous silicon-based optoelectronic devices. To improve the PL stability of PSi and to meet device requirements, it is necessary to change the PSi surface structure. Many surface modification methods have been employed to improve PL [3]. One of these methods is the passivation of PSi using various techniques such as electrodeposition, sputtering, immersion and thermal evaporation [4–7].

Among these techniques, electrodeposition provides the ability to tailor size, shape, and morphology of the noble metallic nanoparticles deposited under a set of well controlled synthesis parameters [8,9]. Among noble metals, silver has become indispensable in many applications thanks to narrow plasmon resonance and an inexpensive noble metal with anti-bacterial action [10,11]. It is also important to note that the shape and size of Ag nanostructures have a significant effect on optical properties, so efficient control of these is of great importance. However, the growth mechanism of different Ag nanostructures, such as nanoparticle, dendritic Ag, etc., prepared by using electrodeposition has not been fully explored. Apart from synthesize of Ag nanostructures, most of publications particularly include Ag nanoparticles/dendrite used for enhancement of Raman signals [12–15], but a limited number of studies focused on to intensify the PL signal of PSi/Ag [7,16,17]. We have used Ag to modify surface of PS samples due to unique characteristics, such as chemical stability, excellent adhesion to substrates and high conductance. We have expected the potential use of PSi/Ag as an optical material in material science and new silicon-based optoelectronic devices with optimization of the electrochemical deposition parameters such as deposition time and concentration of electrolyte.

In this study, we have synthesized three different Ag structures, such as nanoparticle, dendrite and microparticle, by a simple electrochemical method in aqueous solution

* e-mail: alper.cetinel@ege.edu.tr

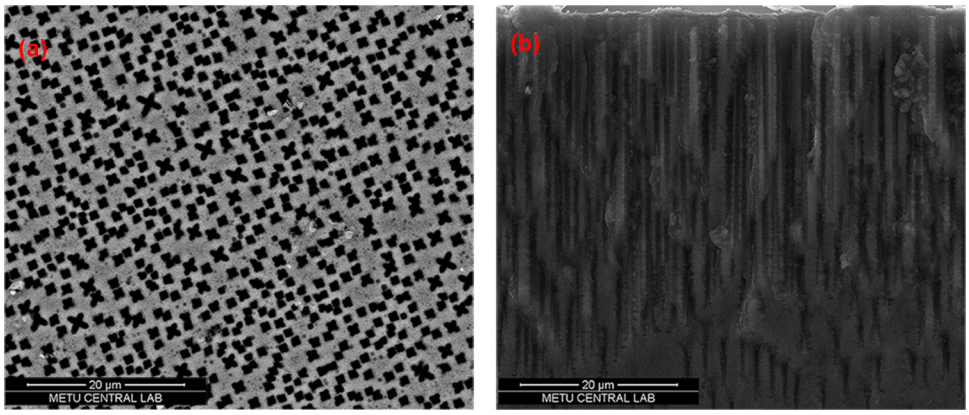

Fig. 1. FE-SEM images of a PSi sample/PSi substrate prepared in 20% HF concentration at 60 mA/cm^2 for 30 min by using the anodization method. (a) top-view, (b) cross-section image.

of $AgNO_3$ and boric acid. We have also investigated how structural and morphological properties of PSi/Ag nanostructures vary with the silver nitrate ($AgNO_3$) concentration and deposition time. The growth mechanism of Ag structures has been also discussed. We have mainly focused on the effect of Ag structures and deposition parameters on photoluminescence properties of PSi/Ag materials. The mechanism of PL emission from PSi/Ag was analysed based on quantum confinement effect and surface effects. It has been found that the electrodeposition technique is low-cost, fast and reproducible method as compared to our previously reported method [7]. The characterizations carried out by using a field emission scanning electron microscopy (FE-SEM), X-ray diffraction (XRD) and PL measurements.

2 Experimental

Phosphorous doped, double-sided polished n-type Si wafer with (100) orientation and 1–10 Ωcm resistivity was used to obtain porous Silicon (PSi) substrate via anodization method. Anodization method was carried out using Teflon tank with Silicon wafer anode and Platinum wire cathode in HF solution (Merck, 40%)/Ethanol (Merck, EMSURE, 99.8%) (1:1). The applied current density was selected as a constant 60 mA/cm^2 for 30 min with backside illumination.

The silver deposition was carried out in dark with a two-electrode system at room temperature in an aqueous solution $AgNO_3$. The anode (working electrodes) and cathode (counter electrodes) were PSi substrate and platinum wire, respectively. The electrodeposition was carried out at 0.3 mA/cm^2 in the aqueous solution of $AgNO_3$ (Ames Goldsmith Limited, UK, 99.5%) with concentration of 1, 5 and 10 mM, and 0.4 M H_3BO_3 (Merck, EMSURE) under stirring conditions ($\omega = 500$ rpm) after reversing the polarization direction. The electrodeposition durations were varied from 60 to 900 s. After deposition, PSi/Ag samples were rinsed with distilled water.

Surface morphologies of PSi/Ag nanostructures were investigated using a field emission scanning electron microscopy system (FE-SEM, QuantaFEG). X-ray diffraction (XRD) patterns of PSi/Ag samples were obtained using a Philips X'Pert Pro X-Ray Diffraction system employing a CuKα radiation ($\lambda = 0.15418$ nm). The PL spectra were recorded using an S&I MonoVista system employing an Ar-Ion laser with 488 nm wavelength emission, a 750 mm focal length Princeton Instruments monochromator with a 150 gr, and a high-resolution CCD camera array for a multichannel detection.

3 Results and discussion

3.1 SEM analyses

SEM images of the cross section and the surface of a freshly prepared PSi substrate are presented in Figure 1. The average pore diameter of PSi substrate, which has a high porosity (75%), is about 850 nm obtained from the SEM image. These pores can be classified as macropores [18]. The pores are straight, but pore walls have considerably rough morphologies. The average depth of the pores in PSi layer is about 50 µm with a columnar structure perpendicular to the Si surface. The pore channels are not interconnected with each other as seen in Figure 1.

Figure 2 shows the effects of $AgNO_3$ concentration on the sizes and shapes of nanostructures forming on the surface of PSi/Ag samples. The SEM images of the PSi/Ag surface, prepared at 0.3 mA/cm^2 for 300 s at 1, 5, 10 mM $AgNO_3$ concentrations, are presented. Based on the values of the concentration of $AgNO_3$, it can be seen in Figure 2, three different types of Ag structures were formed. SEM analyses have shown that nanoparticle clusters of 10–150 nm in diameter and short and thin (several nm) nanorods/branched nanostructures formed at 1 mM concentration, whereas nanoparticle clusters of 20–300 nm in diameter and longer and thicker (several hundred nm) nanowires/branched nanostructures were found at 5 mM concentration. Increasing the $AgNO_3$ concentration to 10 mM, silver aggregate growth presents a dense structure of micrometre-size particles.

The SEM images in Figures 3a–3d show the morphological evolution of silver nanostructures prepared at 1 mM $AgNO_3$ concentration for 60, 120, 180, 600 and 900 s of deposition time, respectively. As can be seen in Figure 3a, in

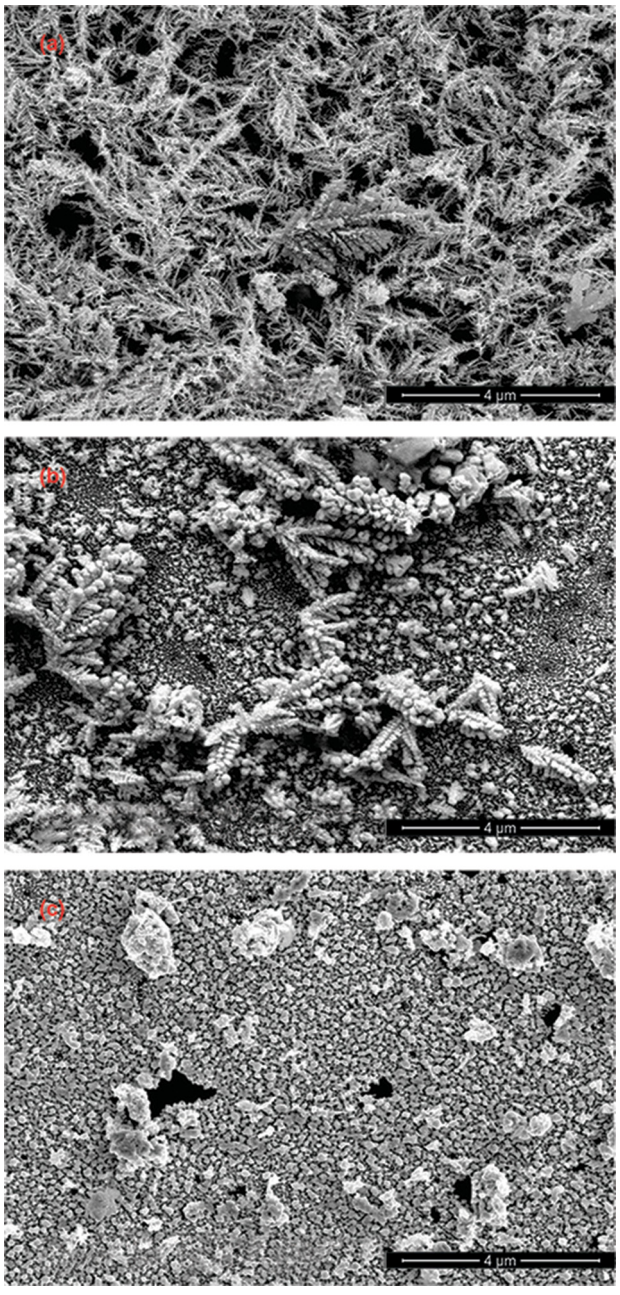

Fig. 2. FE-SEM images of PSi/Ag nanostructures deposited at 0.3 mA/cm^2 for 300 s (a) 1 mM, (b) 5 mM, (c) 10 mM concentration of $AgNO_3$.

the case of 60 s deposition time, the resulting Ag nanoparticles are very small and nonuniform. For 120 and 180 s of deposition time, nanoparticles with a diameter of 10–20 nm have been observed almost all over the surface of the sample, while cluster-branched nanostructures growing on these nanoparticles only have been seen in specific regions of the surface. For 600 s, the branched nanostructures merged to form a thicker, longer structure and spread out over much wider areas. Increasing the deposition time to 900 s, nanoparticles growing on the surface increased in diameter (30–40 nm) and nanostructures grown on these structures appeared as nanorods (100 nm).

Figure 4 demonstrates the transition from nanoparticles to dendritic growth of Ag nanostructures at 5 mM $AgNO_3$ concentration for 60, 120, 180, 600 and 900 s of deposition time, respectively. For 60 s, some dendritic nuclei of silver were found on the rough surface of the PSi along with a few smaller dendritic nanostructures. When the deposition time is 120 s, aggregated Ag nanoparticles with nano-sized Ag dendrites formed on the surface of the PSi/Ag. Increasing the deposition time to 180 s, the dendritic Ag nanostructures became thicker and spread out over larger areas on the surface of the PSi/Ag. When the deposition time increased to 600 s, the multibranched Ag dendrites with a complex morphology formed on the surface, as seen in Figure 4c. The thicknesses of these structures are several hundred nanometres, while their lengths reach several micrometres. When the deposition time was raised to 900 s, thin film layer of Ag particles with a size of 100–200 nm with some dense Ag dendrites were observed on the surface of PSi/Ag. When we compare the silver structures formed at 1 and 5 mM, it is seen that the size of the silver structures increase with increasing concentration.

When the concentration of $AgNO_3$ was 10 mM, no Ag dendrites were formed on the surface of PSi/Ag regardless of deposition time, as seen in Figure 5. Only, a dense structure of micrometre-size Ag particles is seen in Figure 5. It has been also found that the structure of micrometre-size Ag particles is composed of agglomerates of smaller submicron particles that have merged together. Figure 5 demonstrates that with increasing deposition time from 60 to 900 s, the diameter of Ag particles is increased to values in the range of 1–5 µm, due to aggregation of particles on the surface of PSi/Ag. We have prepared our PSi/Ag samples in a wide range of parameters in this study, compared to our previous study [7]. For each $AgNO_3$ concentration (1, 5 and 10 mM), SEM images of all samples (6 samples per concentration) have shown that PSi/Ag samples have similar structure and shape at a constant current density, confirming the high reproducibility and repeatability of these results. Depending on the deposition time, only in terms of size, the change in the structure of our samples has observed from SEM analysis. All the experimental samples investigated in our study have been prepared two or three times.

In our study, to obtain Ag nanostructures, electrochemical deposition was used under constant current density. Compared to immersion method, the most important difference of our study is the current density [15,19,20]. Although Ag nanostructures/or dendrites have been obtained in the long immersion times, it is seen in SEM analysis that with the effect of current density, the Ag nanostructures/or dendrites occur in the shorter deposition times in our study. It is clear that the applied current acts as a main driving force for the movement of ions in an aqueous solution of $AgNO_3$ and H_3BO_3. Surface SEM analyses indicate that the formation of silver structures is dominated by both $AgNO_3$ concentration and deposition time. For 1 and 5 mM $AgNO_3$ concentrations, the growth mechanism of Ag dendrite nanostructures may be explained by using diffusion-limited aggregation (DLA) model [9,21]. At the initial stage of electrodeposition, Ag^{2+}

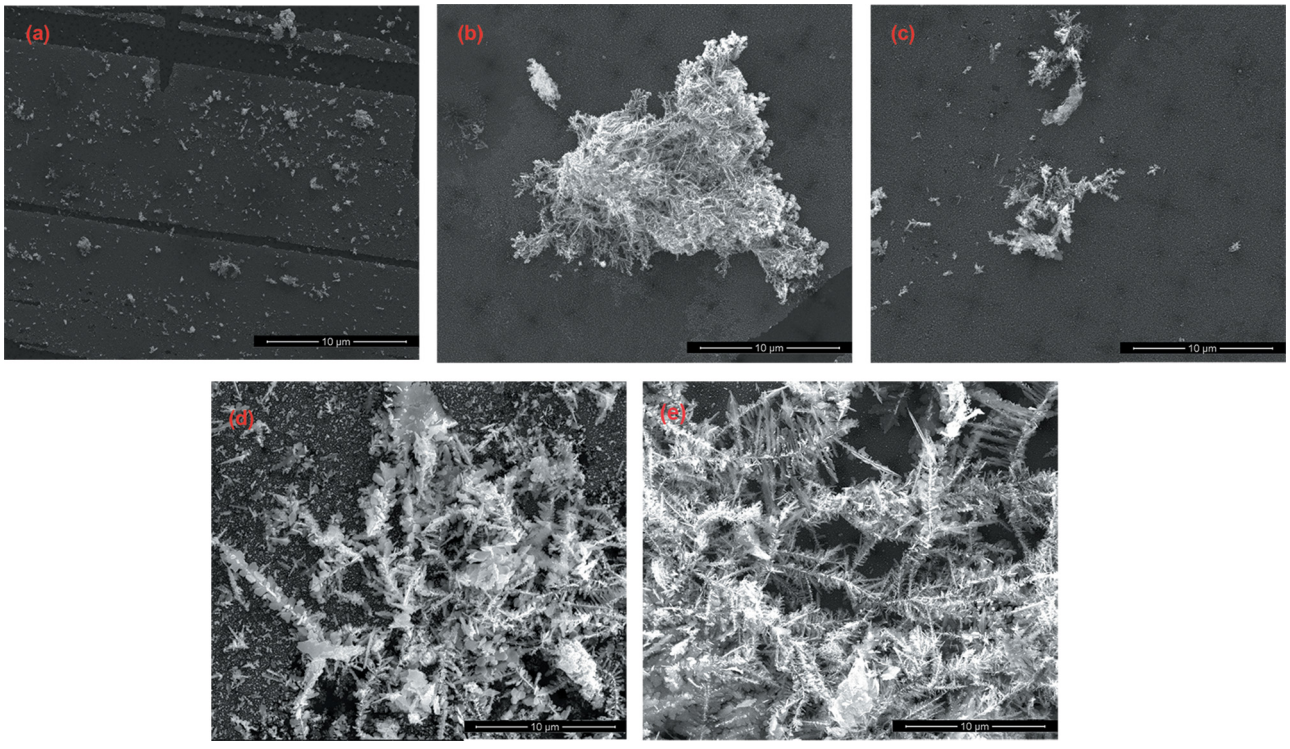

Fig. 3. FE-SEM images of PSi/Ag nanostructures deposited at 0.3 mA/cm^2 in 1 mM concentration of $AgNO_3$ for (a) 60 s, (b) 120 s, (c) 180 s, (d) 600 s and (e) 900 s.

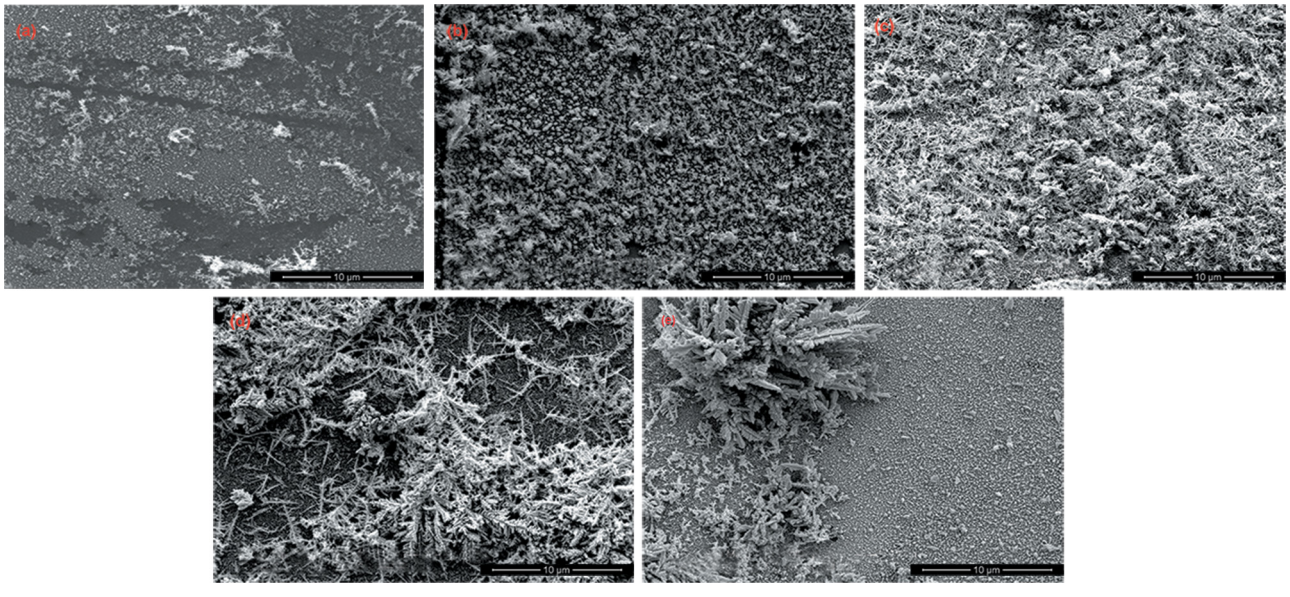

Fig. 4. FE-SEM images of PSi/Ag nanostructures deposited at 0.3 mA/cm^2 in 5 mM concentration of $AgNO_3$ for (a) 60 s, (b) 120 s, (c) 180 s, (d) 600 s and (e) 900 s.

ions accept electrons to form Ag nanoparticles on the porous silicon. As the reaction progress, the additional silver nanoparticles are synthesized at the same time. The additional particles grow along the silver trunk to form new branches. As the reaction continues, branches grow bigger, thicker as well as denser and finally become interconnected to form the most ordered, well oriented silver dendritic structures. For a 10 mM $AgNO_3$ concentration, the deposition of Ag microparticle clusters on PSi follows 3D island (Volmer–Weber) growth mechanism [6,22]. At the initial stage of electrodeposition, a highly uniform layer, composed of large crystalline silver particles were

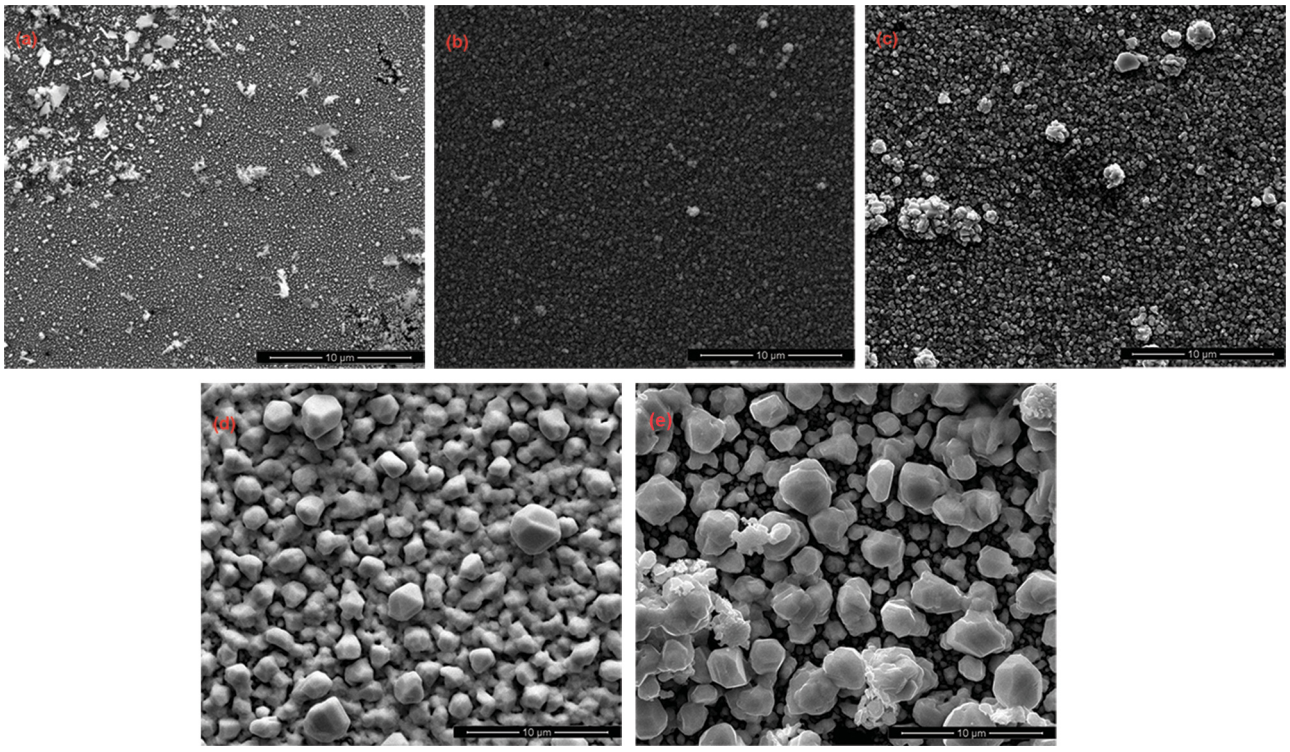

Fig. 5. FE-SEM images of PSi/Ag nanostructures deposited at 0.3 mA/cm^2 in 10 mM concentration of $AgNO_3$ for (a) 60 s, (b) 120 s, (c) 180 s, (d) 600 s and (e) 900 s.

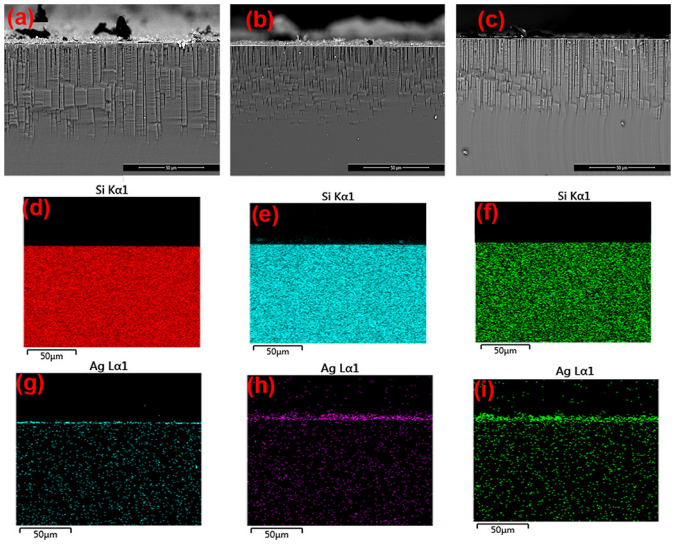

Fig. 6. The cross-section FE-SEM images of PSi/Ag nanostructures deposited at 0.3 mA/cm^2 for 300 s. (a) 1 mM, (b) 5 mM and (c) 10 mM $AgNO_3$ concentration. Mapping of EDAX analyses from the cross-section FE-SEM images of PSi/Ag nanostructures have been also presented in (d), (e), and (f) Si content, and (g), (h), and (i) Ag content in 1, 5, and 10 mM concentration, respectively.

formed due to the high silver nitrate concentration. This process is called instantaneous nucleation. With increasing deposition time, micron-sized Ag particles, composed of agglomerates of sub-micron Ag particles, form thick and continuous layer on PSi. Consequently, based on the SEM analyses, the morphology of Ag structures electrodeposited on PSi is found to be highly dependent on the concentration of the $AgNO_3$ solution, while the deposition time is found to have remarkable influence on the size and formation of branched Ag dendrites. It should be important to note that since the diameters of the nanoparticles obtained in this study are quite large compared to the pore diameters of the porous silicon, only the effects of the Ag nanostructures on the PSi surface has been investigated in the XRD and photoluminescence analyses.

Figure 6 shows the cross-sectional SEM images and mapping EDAX analysis of PSi/Ag samples deposited at 0.3 mA/cm^2 for 300 s under 1, 5, and 10 mM $AgNO_3$ concentration. It should be noted that some larger particles observed in the images may have fallen during the cleavage from the surface of PSi/Ag. We can see from the images that at 1 mM $AgNO_3$ concentration, some pores are partially filled, but most of the pores are empty. Cross-section images reveal that at 5 and 10 mM $AgNO_3$ concentration, the silver crystals appear to be on the surface only, whereas no silver could be observed inside the pores. Thus, increasing the concentration of the $AgNO_3$ leads to the formation of a highly uniform layer, composed of larger crystalline silver particles, as can be seen from SEM images.

3.2 XRD analyses

The typical XRD pattern of as-prepared Ag nanostructures for samples, which were fabricated in 1, 5 and 10 mM $AgNO_3$ concentrations at current density of 0.3 mA/cm^2 with varying deposition times 120, 180, 600 and 900 s, are

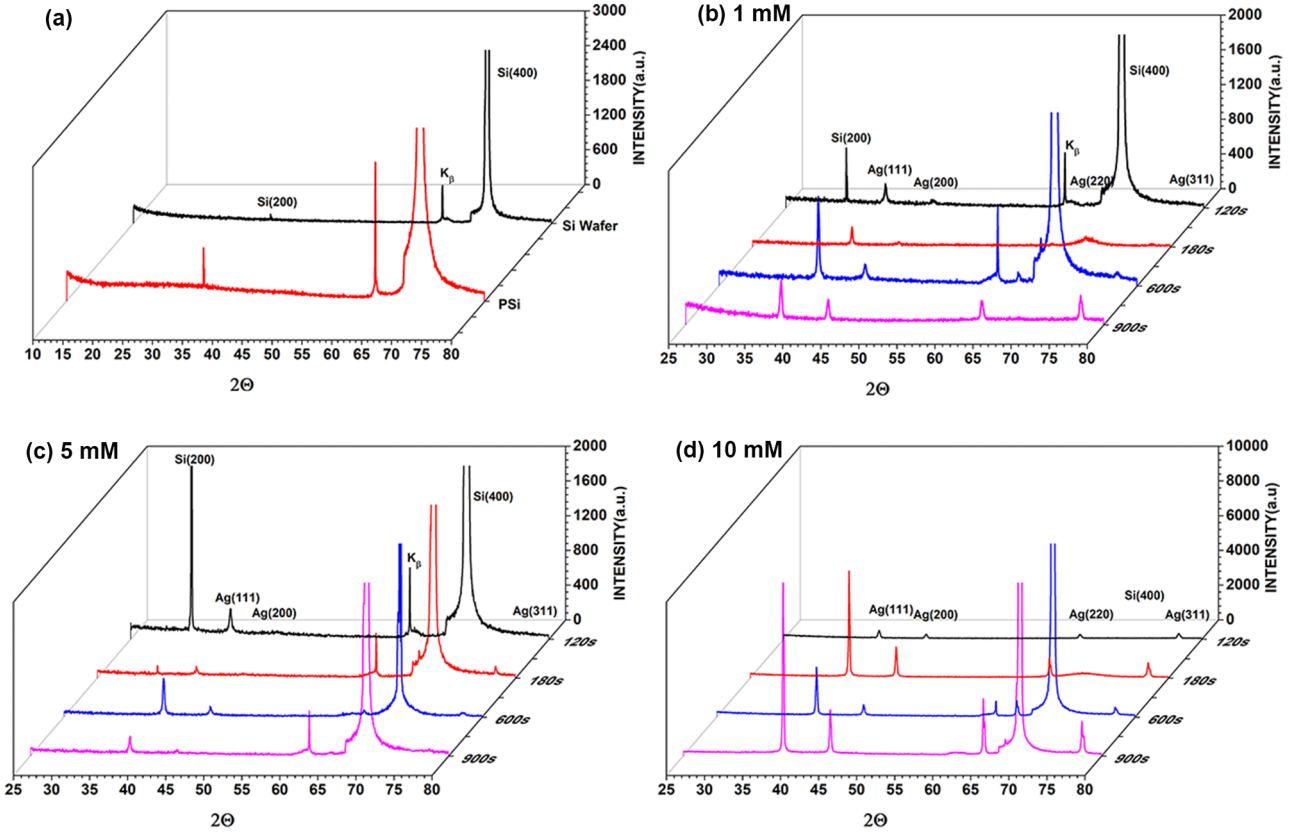

Fig. 7. (a) The XRD patterns of n-type Si wafer and reference as prepared PSi are drawn for comparison. The XRD patterns of PSi/Ag nanostructures prepared at current density of 0.3 mA/cm^2 with varying deposition times 120, 180, 600 and 900 s, (b) 1 mM, (c) 5 mM and (d) 10 mM concentrations of $AgNO_3$.

shown in Figure 7. XRD patterns of the n-type Si wafer and reference as prepared PSi are also drawn for comparison (Fig. 7a). XRD analyses reveal that four diffraction peaks, indexed to the (111), (200), (220) and (311) planes of the face centered cubic (FCC) structure of silver, were in agreement with the JCPDS file no. 4-0781 for silver [8,9]. Apart from the Ag diffraction peaks, the Si (400) peak seen at 70° is the main peak of the n-type Si (100) substrate. Furthermore, the peak observed at 61.7° belongs to the K_β radiation diffracted from the Si (400) planes [23]. Although macro morphology of the obtained Ag nanostructures is very different, it can be observed some similarities at the micro level among the Ag nanostructures obtained from 1, 5 and 10 mM $AgNO_3$ concentration. Basically, the spherical Ag grains are a characteristic of all types of the Ag nanostructures and the XRD patterns are very close to the Ag standard. For all $AgNO_3$ concentrations and deposition times, the dominant peak for Ag is (111) plane, which has the lowest surface energy, as seen in Figures 7b–7d. XRD results indicate that as the deposition time and $AgNO_3$ concentration increase, the intensity of (111) plane of FCC silver increases due to the gradual increase in the number of Ag structures. This result shows that the degree of crystallization of the micro-sized Ag nanostructures is much better than those of the Ag nanoparticles and dendritic structure. The ratios of intensities of diffraction peaks are also calculated from XRD data and listed in Table 1. The peak intensity ratios of the (111) to (200) diffractions, given in Table 1, are higher than that of polycrystalline Ag (2.5). The higher peak intensity ratio is due to an increase in the grain size of the Ag particles in the (111) plane on PSi, with increasing deposition time and $AgNO_3$ concentration. The crystallite size is calculated by using Debye–Scherrer's formula [24]. As can be seen in Figure 7, large crystallite size causes sharp reflections, whereas small size leads to broader reflections, which is consistent with the SEM analyses.

3.3 Photoluminescence analyses

The PL spectra of the reference PSi sample and PSi/Ag samples are illustrated in Figure 8. All PL spectra show the same tendency in which PL intensity decreases as the deposition time increases (Fig. 8, Tab. 2). As already mentioned, SEM analyses have revealed that the density of silver is low, and the growth of silver cluster randomly occurs on the PSi surface at 60 s of deposition time for 1 and 5 mM $AgNO_3$ concentrations. However, the effect of silver deposition on PL intensity of these samples is significant and the PL intensities of these samples are slightly higher than that of the reference PSi sample. It can be seen in

Table 1. The effects of $AgNO_3$ concentration and deposition time on the size of Ag particle and the peak intensity ratios of the (111) to (200) diffractions.

$AgNO_3$ concentration (mMol)	Deposition time (s)	Ratio of intensities (111)/(200)	Size of the Ag particle in (111) plane (nm)
1	120	3.77	22.40
	180	3.81	32.90
	600	4.31	30.50
	900	1.74	31.40
5	120	5.10	21.70
	180	2.83	22.50
	600	3.50	27.80
	900	4.18	29.00
10	120	1.74	34.30
	180	3.42	40.50
	600	4.01	37.00
	900	4.28	42.10

Figure 8a that at 1 mM $AgNO_3$ concentration, the highest PL enhancement of about ~2.7 times obtained from PSi/Ag sample, prepared at 120 s of deposition time, as compared with a reference as prepared PSi. When the deposition time increases from 120 to 900 s, the PL intensity of PSi/Ag samples decreases about ~4.2 times, compared to that of the reference PSi. It is found that the PL peak of PSi/Ag for 120 s was blue-shifted (22 nm in wavelength) with respect to the reference PSi, as seen in Figure 8a. It is also observed that with increasing deposition time, the PL peaks of PSi/Ag samples were consistently red-shifted (25 nm in wavelength), compared to that of the reference PSi. In a similar manner, for 5 mM $AgNO_3$ concentration, a substantial improvement of the PL intensity (about ~2.1 times) is noticed for PSi/Ag sample, deposited at 120 s, as compared with reference PSi (Fig. 8b). As the deposition time increases from 120 to 900 s, PL intensity decreases about ~4.0 times with respect to the reference PSi. It is also seen in Figure 8b that the PL peak of PSi/Ag for 120 s was blue-shifted (16 nm in wavelength), whereas the position of PL peaks shifted towards the longer wavelengths (red) with the increasing deposition time, as compared with the reference PSi. When the concentration of $AgNO_3$ is 10 mM, PL intensities dramatically decrease about 1.5–5 times compared with reference PSi due to forming a dense structure of micrometer-size Ag particles, that suppresses light emission significantly (Fig. 8c).

It is well known that the novel metallic nanoparticles show an optical absorption peak in the visible wavelength as a particular characteristic. Mostly, in size ranges between about 10 and 100 nm, localized surface plasmons determine the optical properties of the nanoparticles. As the mean diameter of the Ag nanoparticle increased, the peak in the absorption spectra showed a red shift, because of surface plasmon resonance [25]. The surface plasmon absorption of the Ag nanostructures is observed between 390–550 nm in the optical absorption spectra of Ag. Since the PL measurement carried out with excitation wavelength of 488 nm in this study, the UV band emission of Ag nanostructures is not observed in the PL spectra of all samples.

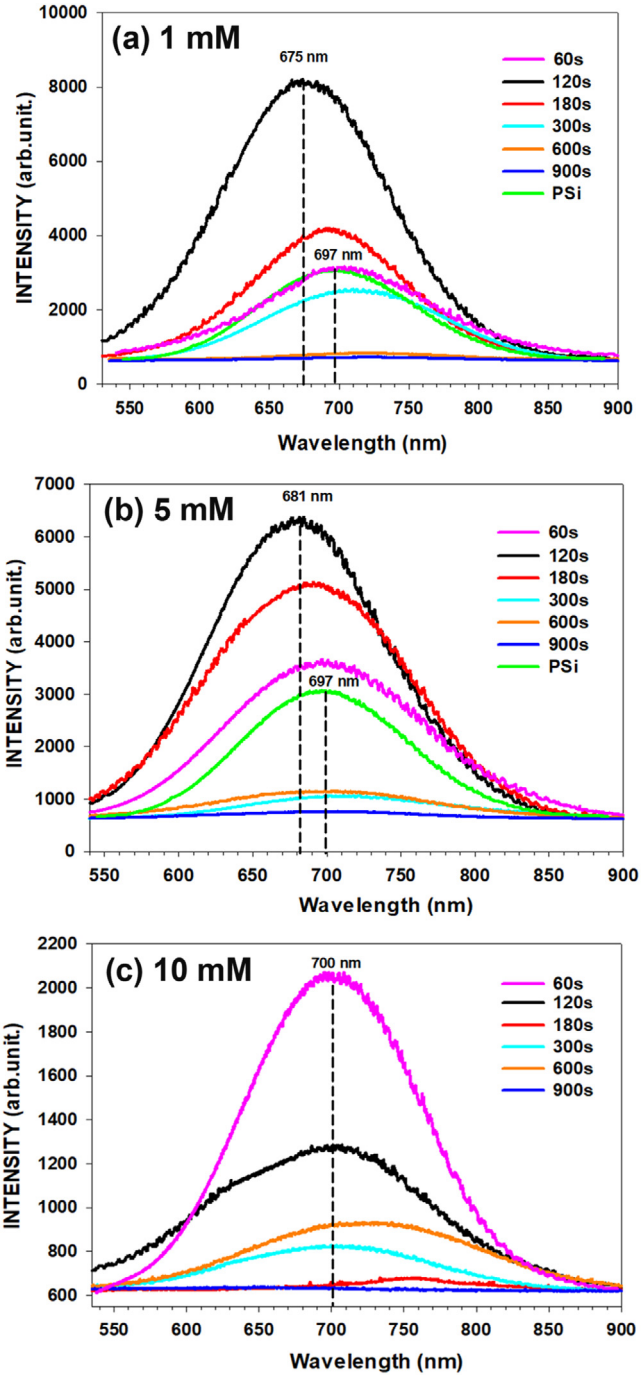

Fig. 8. Room temperature PL spectra of PSi/Ag nanostructures prepared at current density of 0.3 mA/cm^2 for varying deposition times (60–900 s). (a) 1 mM, (b) 5 mM and (c) 10 mM concentration of $AgNO_3$ (The PL spectrum from the reference as prepared PSi sample is also shown for comparison).

Table 2. Effect of the $AgNO_3$ concentration and deposition time on PL characteristics of PSi/Ag nanostructures.

Sample	$AgNO_3$ concentration (mMol)	Deposition Time (s)	PL intensity (arb.un.) (as-prepared)	PL peak maximum (nm) (±1 nm) (as-prepared)
Porous silicon	–	–	3050	697
PSi/Ag	1	60	3141	700
		120	8200	675
		180	4160	692
		300	2455	709
		600	811	721
		900	724	722
	5	60	3647	697
		120	6385	681
		180	5089	691
		300	1055	712
		600	1139	708
		900	754	721
	10	60	2055	700
		120	1282	701
		180	680	–
		300	823	706
		600	928	728
		900	630	–

Based on the PL analyses, we can say that the Ag nanoparticles and dendritic structures could modify the surface electronic structure via creating the new radiative recombination centers and changing the bond structure from Si–H to Si–Ag and/or Si–O–Ag bonds to saturate dangling bonds. It should be important to note that PL spectra of all samples exhibit a similar broad emission in the visible range, which is known as an S-band. To explain S-band, various models, including the quantum confinement model and surface states model have been studied over the past few decades [1,26,27]. However the quantum confinement model widely accepted, there is still controversy about the nature of PL from PSi deposited with noble metal nanostructures [3,4,7,10,16,28,29]. PL from noble metal was first observed by Mooradian and was attributed to radiative recombination of excited electrons and the hole in the sp-band and d-band, respectively [30]. Furthermore, Apell and Monreal developed a theoretical model to explain the photoluminescence from the roughened surface of noble metals [31]. Boyd et al. [32] carried out an extensive study on the PL from noble metal, such as silver and gold, to determine the relation between spectral peaks and the interband recombination transition. Wilcoxon et al. [33] pointed out that the radiative recombination transition is responsible for the PL from nanocluster noble metals. More recently, Hamzah et al. [34] speculated that PL mechanism of Ag nanoparticles may result from the direct recombination of electrons and holes. They also found that as the radiative recombination of electron and hole was reduced, PL intensity decreased [34]. According to these studies [30–34], the origin of PL from noble metals was due to the radiative recombination of an electron-hole pair. Briefly, i) the incident photons are absorbed by the d-band electrons, and then ii) the photon energy promotes these excited electrons in occupied d bands to above Fermi level in sp-band. iii) rapid relaxation by phonon scattering produces the observed PL from noble metals. Comparing all PSi/Ag samples and the reference PSi sample, we can conclude that the PL from PSi/Ag should be originated from the combination of QCE and surface effects. Therefore, high PL enhancement of PSi/Ag can be explained by the radiative recombination of sp-band electrons with d-band holes, which are related to Si–Ag and/or Si–O–Ag bonds, whereas the blue shift in PL peak is due to the QCE which is related to the confinement of the optical phonons in the nanocrystalline Si crystallites in pore walls of PSi matrix. On the other hand, PL analyses have revealed that as the Ag density and the particle size increase with increasing deposition time and the concentration of $AgNO_3$, PL intensities significantly decrease and the PL peaks is found to shift towards higher wavelengths (red shift), which mean the band gap decreases due to sp–d exchange interactions as discussed by Kondow et al. [25], compared to that of the reference PSi. The decrease in PL intensities is due to increased in the number of non-radiative centers with the increasing Ag density, causing a reduction in the probability of electron-hole recombination process. This is widely known as auto-extinction phenomenon [35]. Consequently, we can say that the concentration of $AgNO_3$ and deposition time significantly affect the shape and size of the silver particles, resulting in an increase or a decrease in the intensity of PL of PSi/Ag samples.

4 Conclusion

Silver deposition on the PSi templates via electrodeposition method was carried out at a current density of 0.3 mA/cm^2 at three different concentrations of $AgNO_3$ (1, 5 and 10 mM), and at six different deposition times (60, 120, 180, 300, 600 and 900 s). According to the SEM analyses, the Ag deposition is in the form of Ag nanoparticle clusters with a small amount of short nanorod/dendrite of Ag nanostructures at 1 mM $AgNO_3$, but for 5 mM $AgNO_3$, Ag nanoparticle clusters with a longer and thicker Ag nanowire/dendrite occur. At 10 mM $AgNO_3$, Ag nanostructures were form only as spherical microparticles at the whole current densities and deposition times. XRD analyses have revealed that Ag nanoparticles and dendrites formed in the PSi matrix by electrodeposition method are only in the cubic FCC Ag structure. It is also found that the degree of crystallization of Ag structures increases with increasing concentration from 1 to 10 mM. PL analyses have shown that for 1 mM $AgNO_3$, PSi/Ag sample, prepared at 120 s, have the highest PL intensity (~2.7 times) than both those of the reference PSi and all the other PSi/Ag samples. The increase in the PL intensity of PSi/Ag sample at 120 s is due to Ag nanoparticles create the new radiative recombination centers and the confinement of the optical phonons in the nanocrystalline Si crystallites in pore walls of

PSi matrix. It is found that the PL intensity is completely quenched for the samples with 10 mM $AgNO_3$ at the whole current density and deposition times. In conclusion, this study reveals that the structural and photoluminescence properties of PSi/Ag samples significantly depend on the deposition time and concentration of $AgNO_3$. These results suggest that the PSi/Ag sample with finely controlled atomic-scale structure, is a good candidate for the potential applications in optoelectronic and sensor devices.

This work was supported by the Ege University, Research Project Foundation (Project no: 2013FEN058).

References

1. A.G. Cullis, L.T. Canham, P.D.J. Calcott, Appl. Phys. Rev. **82**, 909 (1997)
2. M.A. Tischler, R.T. Collins, J.H. Stathis, J.C. Tsang, Appl. Phys. Lett. **60**, 639 (1992)
3. J. Sun, Y.W. Lu, X.W. Du, S.A. Kulinich, Appl. Phys. Lett. **86**, 1 (2005)
4. Y.W. Lu, X.W. Du, J. Sun, X. Han, S.A. Kulinich, J. Appl. Phys. **100**, 063512 (2006)
5. M.E. Raypah, N.M. Ahmed, Mater. Sci. Semicond. Process. **31**, 235 (2015)
6. E. Nativ-Roth, K. Rechav, Z. Porat, Thin Solid Films **603**, 88 (2016)
7. A. Cetinel, M. Ozdogan, G. Utlu, N. Artunç, G. Sahın, E. Tarhan, Surf. Rev. Lett. **24**, 1750074 (2017)
8. C.L. Liang, K. Zhong, M. Liu, L. Jiang, S.K. Liu, D.D. Xing, Nano-Micro Lett. **2**, 6 (2010)
9. M.V. Mandke, S.H. Han, H.M. Pathan, CrystEngComm **14**, 86 (2012)
10. B. Polyakov, R. Zabels, A. Sarakovskis, S. Vlassov, A. Kuzmin, Phys. Scr. IOP Publishing **90**, 2 (2015)
11. T. Kim, G.B. Braun, Z.G. She, S. Hussain, E. Ruoslahti, M.J. Sailor, ACS Appl. Mater. Interfaces **8**, 30449 (2016)
12. X.K. Meng, S.C. Tang, S. Vongehr, J. Mater. Sci. Technol. **26**, 487 (2010)
13. W. Ye, C. Shen, J. Tian, C. Wang, L. Bao, H. Gao, Electrochem. Commun. **10**, 625 (2008)
14. S. Xie, X. Zhang, D. Xiao, M.C. Paau, J. Huang, M.M.F. Choi, J. Phys. Chem. C **115**, 9943 (2011)
15. H. Lin, J. Mock, D. Smith, T. Gao, M.J. Sailor, J. Phys. Chem. B **108**, 11654 (2004)
16. T. Nakamura, S. Adachi, J. Lumin. **132**, 3019 (2012)
17. H.Y. Zhang, X.Y. Lv, Z.H. Jia, Adv. Mater. Res. **486**, 239 (2012)
18. A. Cetinel, N. Artunç, G. Sahin, E. Tarhan, Int. J. Mod. Phys. B **29**, 1550093 (2015)
19. F. Giorgis, E. Descrovi, A. Chiodoni, E. Froner, M. Scarpa, A. Venturello, Appl. Surf. Sci. **254**, 7494 (2008)
20. A.Y. Panarin, S.N. Terekhov, K.I. Kholostov, V.P. Bondarenko, Appl. Surf. Sci. **256**, 6969 (2010)
21. S. Kaniyankandy, J. Nuwad, C. Thinaharan, G.K. Dey, C.G. S. Pillai, Nanotechnology **18**, 125610 (2007)
22. G. Oskam, J.G. Long, A. Natarajan, P.C. Searson, J. Phys. D: Appl. Phys. **31**, 1927 (1998)
23. G. Utlu, N. Artunç, S. Budak, S. Tari, Appl. Surf. Sci. **256**, 5069 (2010)
24. J.H. Adawyia, M.A. Alwan, A.J. Allaa, Microporous Mesoporous Mater. **227**, 152 (2016)
25. F. Mafune, J. Kohno, Y. Takeda, T. Kondow, J. Phys. Chem. B **104**, 9111 (2000)
26. L. Pavesi, R. Turan, *Silicon Nanocrystals*, 1st edn. (Wiley-VCH Verlag GmbH & Co. KGaA, Weinheim, 2010)
27. P.D.J. Calcott, K.J. Nash, L.T. Canham, M.J. Kane, D. Brumhead, J. Phys.: Condens. Matter **4**, 91 (1993)
28. S.N.A. Jenie, S.E. Plush, N.H. Voelcker, Pharm. Res. **33**, 2314 (2016)
29. H. Hu, H. Duan, J.K.W. Yang, Z.X. Shen, ACS Nano **6**, 10147 (2012)
30. S. Link, M.A. El-sayed, Int. Rev. Phys. Chem. **19**, 409 (2000)
31. P. Apell, R. Monreal, S. Lundqvist, Phys. Scr. **38**, 174 (1988)
32. G.T. Boyd, Z.H. Yu, Y.R. Shen, Phys. Rev. B **33**, 7923 (1986)
33. J.P. Wilcoxon, J.E. Martin, F. Parsapour, B. Wiedenman, D. F. Kelley, J. Chem. Phys. **108**, 9137 (1998)
34. M. Hamzah, M.S.V. Khenfouch, J. Mater. Sci.: Mater. Electron. **28**, 1804 (2017)
35. M. Rahmani, A. Moadhen, M.A. Zaïbi, H. Elhouichet, M. Oueslati, J. Lumin. **128**, 1763 (2008)

Cite this article as: Alper Cetinel, Nurcan Artunç, Enver Tarhan, The growth of silver nanostructures on porous silicon for enhanced photoluminescence: The role of $AgNO_3$ concentration and deposition time, Eur. Phys. J. Appl. Phys. **86**, 11301 (2019)